HAL
open science

# Micro-mechanical assembly and characterization of high-quality Fabry–Pérot microcavities for the integration of two-dimensional materials

Christoph Rupprecht, Nils Lundt, Matthias Wurdack, Petr Stepanov, Eliezer Estrecho, Maxime Richard, Elena Ostrovskaya, Sven Höfling, Christian Schneider

## To cite this version:

Christoph Rupprecht, Nils Lundt, Matthias Wurdack, Petr Stepanov, Eliezer Estrecho, et al.. Micro-mechanical assembly and characterization of high-quality Fabry–Pérot microcavities for the integration of two-dimensional materials. Applied Physics Letters, 2021, 118 (10), pp.103103. 10.1063/5.0034851 . hal-03735605

**HAL Id: hal-03735605**

**https://hal.science/hal-03735605v1**

Submitted on 25 Aug 2023

**HAL** is a multi-disciplinary open access archive for the deposit and dissemination of scientific research documents, whether they are published or not. The documents may come from teaching and research institutions in France or abroad, or from public or private research centers.

L'archive ouverte pluridisciplinaire **HAL**, est destinée au dépôt et à la diffusion de documents scientifiques de niveau recherche, publiés ou non, émanant des établissements d'enseignement et de recherche français ou étrangers, des laboratoires publics ou privés.

Applied Physics Letters ARTICLE scitation.org/journal/apl

# Micro-mechanical assembly and characterization of high-quality Fabry–Pérot microcavities for the integration of two-dimensional materials

Cite as: Appl. Phys. Lett. **118**, 103103 (2021); doi: 10.1063/5.0034851
Submitted: 23 October 2020 · Accepted: 22 February 2021 ·
Published Online: 10 March 2021

View Online Export Citation CrossMark

Christoph Rupprecht,[1] Nils Lundt,[1] Matthias Wurdack,[2] Petr Stepanov,[3] Eliezer Estrecho,[2] Maxime Richard,[3] Elena A. Ostrovskaya,[2] Sven Höfling,[1] and Christian Schneider[4,a)]

## AFFILIATIONS

[1]Technische Physik and Wilhelm-Conrad-Röntgen-Research Center for Complex Material Systems, Universität Würzburg, D-97074 Würzburg, Am Hubland, Germany
[2]ARC Centre of Excellence in Future Low-Energy Electronics Technologies and Nonlinear Physics Centre, Research School of Physics, The Australian National University, Canberra, ACT 2601, Australia
[3]University Grenoble Alpes, CNRS, Grenoble INP, Intitute Néel, 3800 Gernoble, France
[4]Institute of Physics, University of Oldenburg, 26129 Oldenburg, Germany

[a)]Authors to whom correspondence should be addressed: christian.schneider @uni-oldenburg.de

25 August 2023 08:16:52

## ABSTRACT

Integrating monolayers of two-dimensional semiconductors into optical microcavities is challenging because of the very few available approaches to coat the monolayers with dielectric materials without damaging them. Some strategies have been developed, but they either rely on complicated experimental settings and expensive technologies or limit the achievable cavity quality factors. Thus, high quality Fabry–Pérot microcavities are not widely available to the community focusing on light-matter coupling in atomically thin materials. Here, we detail a recently developed technique to micro-mechanically assemble Fabry–Pérot microcavities. Our approach promotes strong coupling conditions with excitons in atomically thin materials, it does not rely on difficult or expensive technologies, it is reproducible, and it yields microcavities with quality factors approaching 4000. It is ideally suitable for engineering coupled monolayer-cavity systems of advanced complexity in small-scale laboratories.

*Published under license by AIP Publishing.* https://doi.org/10.1063/5.0034851

Atomically thin transition metal dichalcogenide crystals (TMDCs) belong to an emergent class of materials of high relevance for fundamental studies of light-matter interaction, as well as application-oriented research. They combine huge oscillator strength and giant exciton binding energies, making them a particularly interesting platform for cavity quantum electrodynamics. To date, the regime of strong light-matter coupling in optical microcavities has been convincingly demonstrated with single monolayers,[1] even at room temperature.[2–4] In order to integrate a TMDC monolayer into a (planar) Fabry–Pérot microcavity, a variety of approaches have been introduced in the last five years.

Typically, as a first step, a monolayer is placed on a bottom distributed Bragg reflector (DBR) mirror. Subsequently, the monolayer must be capped with some type of dielectric material, and finally a top mirror is deposited. This can be a metallic layer or a DBR. The deposition of metallic layers yields optical resonators with relatively small effective cavity lengths on the order of a few hundred nanometers.[1] Yet, this approach faces intrinsic limitations in achievable Q-factors (typically $Q < 1000$, limited by absorption in the metallic layers) and is, therefore, prohibitive for a wide range of experiments relying on reduced photon leakage, including the implementation of low threshold lasers or exciton-polariton condensates. Deposition of dielectric layers on TMDC monolayers is very challenging since most techniques have a detrimental impact on the luminescence properties of the monolayer itself. Such deposition was tested with atomic layer deposition (ALD),[5] physical vapor deposition (PVD/sputtering), electron beam evaporation (EBE), and plasma-enhanced chemical vapor deposition (PE-CVD).[4] In their default setting, all these techniques damage the monolayer during the deposition process due to a high temperature, the impact of high-energy ions, or a reactive atmosphere.


Published under license by AIP Publishing

The photoluminescence of the monolayers after such deposition is either completely quenched or strongly decreased and broadened as in the case of ALD deposition of $Al_2O_3$. Protective coating of TMDCs with $Ga_2O_3$ is able to overcome these issues,[6] but so far it has not been tested in the microcavity assembly.

Two coating techniques, which only weakly affect the optical properties of the monolayers, were already successfully tested in microcavity implementations. These are spin-coating of poly-methyl-methacrylate (PMMA)[3] and plasma-assisted evaporation (PAE) of $SiO_2$.[7] Both techniques are also compatible with TMDC monolayers encapsulated by hexagonal boron nitrite (h-BN). The successful fabrication of high quality microcavities with embedded TMDC by PAE has been reported in recent works.[7,8] However, the vast majority of research groups do not have access to a state-of-the-art PAE system. Here, we present an alternative approach, which pursues the idea of utilizing DBR mirrors initially deposited on separate substrates. Such DBRs are commercially made by various companies and have been optimized to yield extremely high reflectivity. The top DBR is then simply placed mechanically on top of the bottom DBR with the coated monolayer. While the technique itself has been previously used by us to assemble a full cavity,[8] here we provide much more profound insight into this methodology.

To implement this idea, a TMDC monolayer is transferred onto a $SiO_2/TiO_2$ bottom DBR (10 pairs) terminated with the low refractive index material. This bottom DBR is purchased from Laseroptik GmbH with 129 nm (79 nm) $SiO_2$ ($TiO_2$) layers designed to have the stop band centered at 750 nm with a typical price range on the order of 100€. Next, the monolayer is isolated and transferred onto the DBR with the conventional PDMS stamping method (well documented in the literature[9]) and a home-built transfer stage. To obtain a full cavity, including the cavity spacer and the top DBR, PMMA is spin coated for 60 s with 6000 turns/s to approximately match the $\lambda/2$-condition for the cavity resonance wavelength. The PMMA concentration in its solvent (anisole) needs to be adjusted in order to obtain the correct cavity thickness (details see below). The coated PMMA is baked at a hotplate for 2 min at 165 °C. Importantly, PMMA capping is known not to affect the quality of the monolayer and has been successfully tested with fully encapsulated TMDC monolayers.[3] In stark contrast to non-invasive dielectric capping strategies, such as PAE, it does not rely on expensive equipment.

Next, we put the bottom DBR with a capped monolayer aside and prepare a separate (top) DBR with 8.5 pairs and high refractive index termination. It should be noted, that in our study, the DBR pair numbers are asymmetric, to couple light preferentially toward the top direction (signal detection). Then, we utilize a sharp item (e.g., a small screwdriver) to manually apply moderate pressure and scratches to the surface of the top DBR. This procedure yields fragmentation of the DBR layer coating, and small pieces (10–50 $\mu$m lateral size) separate from the substrate. Since the top DBR is terminated on both sides with $TiO_2$, flipping the mirror by 180° still results in the desired cavity. The separated pieces can be picked up with a PDMS gel stamp and can subsequently be transferred onto the prepared bottom DBR with the same transfer method as for the TMDC monolayers. Importantly, only pieces with an apparently homogenous and flat surface (under inspection with an optical microscope) were transferred to avoid strongly shifting the cavity mode by, e.g., dirt particles on the surface of the top DBR (see, e.g., Fig. S1). The van der Waals force is sufficient to hold both DBRs together. We do not utilize a heated stage or accurately calibrated pressure in the dry stamping process. This process is illustrated in Fig. 1(a), and a microscope image of a full structure is shown in Fig. 1(b) with the arrow pointing toward the transferred mirror on the upper DBR. Figure S1 shows microscope images of the separated DBR pieces on PDMS and of the same pieces transferred onto the PMMA cavity layer.

The dispersion of the cavity photon, which is measured via angle-resolved reflectivity (details on the technique are given in Ref. 10) next to the monolayer, is shown in Fig. 1(c). Our experiment reveals a well-pronounced cavity dispersion, characterized by an effective mass of $1.23 \times 10^{-5} m_e$ with $m_e$ being the free electron mass. The line spectrum at $k = 0$, depicted in Fig. 1(d), features a linewidth of $0.431 \pm 0.021$ meV, corresponding to a cavity Q-factor of $(3.83 \pm 0.22) \times 10^3$. According to the transfer matrix calculation of this structure, the Q-factor of 25000 with an effective cavity length of ~400 nm can be theoretically achieved; however, we believe that we are limited by material inhomogeneities (photonic disorder) in our structures. In the course of this study, we fabricated 9 cavities with Q-factors between 500 and 4600 characterized by broadband reflectivity measurements with 10 $\mu$m spot size.

To assess the photoluminescence properties of our loaded cavities, we plot the outcome of an angle resolved photoluminescence (PL) measurement (sample temperature: 5 K and excitation wavelength: 532 nm) in Fig. 2(a). The cavity was loaded with a monolayer of $MoSe_2$. The primary luminescence feature arises (modeled by the red dashed lines) at an energy ~25 meV below the empty cavity resonance (white dashed line) and can be associated with PL emergent from the lower polariton branch. The upper branch is thermally depleted. Some photoluminescence from the monolayer is funneled through the empty cavity mode and picked up from areas surrounding the monolayer.[11]

In order to directly verify the normal mode coupling in our structure, we conduct temperature-dependent transmission measurements, as shown in Fig. 2(b). The avoided crossing between the two transmission peaks with a Rabi-Splitting of 31 meV occurs at a temperature of 135 K and is a clear-cut demonstration of the strong-coupling regime in our structure. The absorption peaks were modeled within an input-output approach, which is detailed in supplementary section S3. We would like to stress that this sample retained its excellent properties over >30 cooling procedures and a time period of >3 years without a significant change of the PL and reflectivity properties.

The PMMA layer deposited on the bottom DBR acts as a spacer between the DBRs. Its thickness can be varied to adjust the cavity resonance. In order to check the reproducibility, we fabricate a variety of microcavities and reference samples (PMMA layer on $SiO_2$) with different PMMA concentrations. First, we check the physical layer thicknesses of the samples fabricated with different PMMA concentrations using a *Dektak 3030* Profilometer. To get a defined step, we use a razor blade to remove a small area of PMMA. We conduct this measurement at various positions on our reference samples and calculate the average thickness and standard variation. The results, which are plotted in Fig. 3(a), demonstrate a very good and almost linear correlation between the PMMA concentration and layer thickness. Next, we fabricate assembled cavities with the same PMMA concentrations and study the cavity resonance energy. Figure 3(b) depicts the corresponding cavity wavelength resolved by white light spectroscopy. The first

25 August 2023 08:16:52


Published under license by AIP Publishing

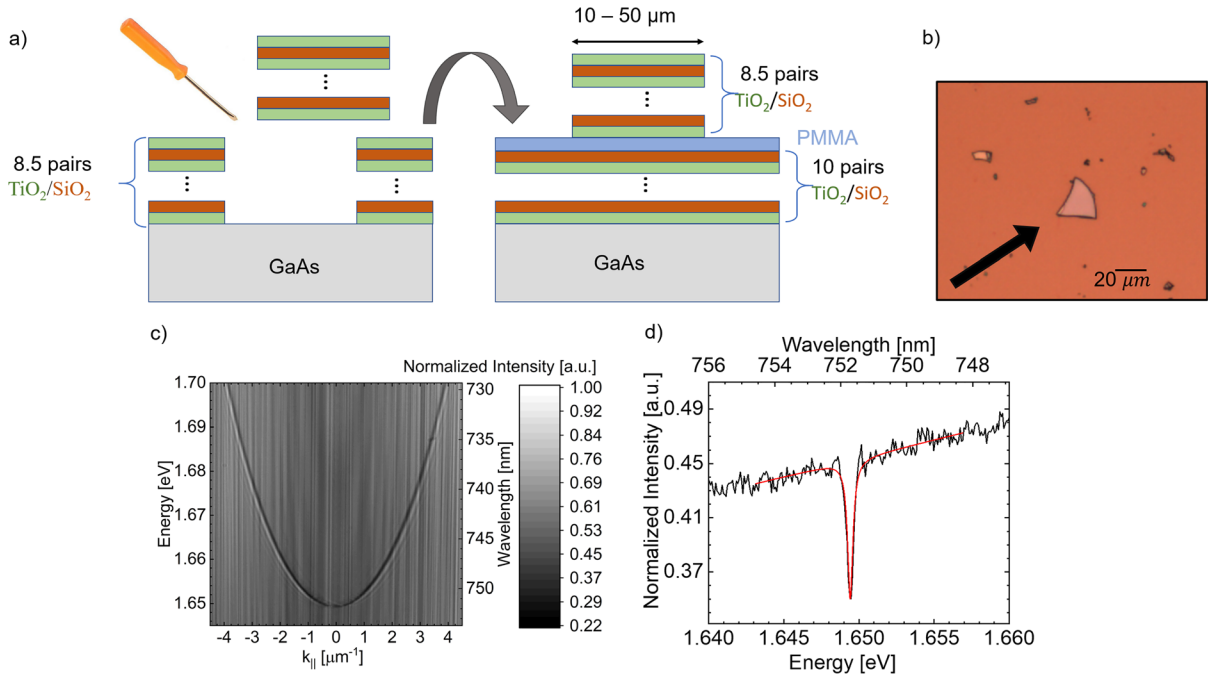


**FIG. 1.** (a) Schematic illustration of the process with a $TiO_2/SiO_2$ DBR. (b) Optical microscope image of a fully assembled structure. (c) High-Q photonic energy dispersion plotted vs the in plane wave vector $k_{||}$. (d) Spectrum at $k = 0\ \mu m^{-1}$ from (c) with Lorentzian fit. The extracted quality factor is $Q = 3827 \pm 222$.

class of devices (data group I) follows the expected linear correspondence between the cavity thickness d (or PMMA concentration, respectively) and optical mode in a Fabry–Pérot cavity.[12] The black line, providing a guide to the eye, visualizes this dependence. The second class of devices (data group II and III) displays a strong deviation from this behavior. To understand this peculiarity, we conduct the transfer matrix simulations of the nominal device structures. As input parameters, we use the measured PMMA thickness [Fig. 3(a)], the

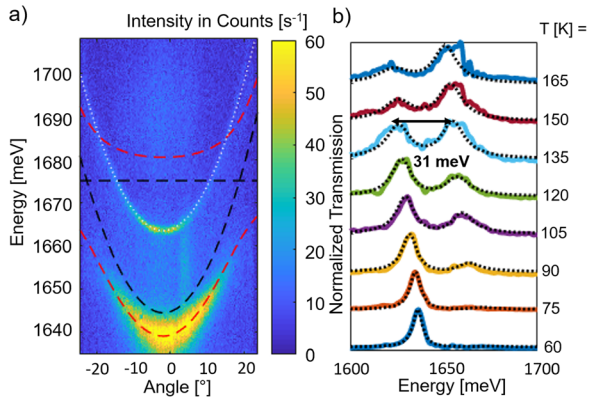


**FIG. 2.** (a) Angle-resolved PL of a cavity loaded with a monolayer $MoSe_2$ at 5 K. The dashed red (black) lines correspond to polariton emission (cavity and exciton resonance). The dashed white line corresponds to the empty-cavity resonance. (b) Temperature-dependent transmission measurements at normal incidence, proving anticrossing of lower and upper polariton branch. The dashed line is extracted from input–output theory.

$SiO_2$ and $TiO_2$ thicknesses provided by the vendor for the DBRs, and the refractive indices of PMMA,[13] $SiO_2$, and $TiO_2$[14,15] (assumed without uncertainties). Error bars in Fig. 3(b) result from the thickness measurement of PMMA. All measured resonance wavelengths can be accurately reproduced by the simulations [orange dots, Fig. 3(b)]. The data points following the approximate linear dependence (data group I) between the concentration and the wavelength correspond to the devices where the top DBR starts on a full $TiO_2$ layer. The cavity resonance for PMMA concentrations of 3.5% is deviating from the linear dependence and corresponds to a higher longitudinal mode of the cavity (data group II). A strong deviation of the resonance for concentrations <2.5% (data group III) can be modeled by devices where the top DBR starts on a $SiO_2$ layer, indicating an intrinsic inaccuracy of mechanical fragmentation of the top DBR. In particular, there is a possibility of the mirror breaking at the $TiO_2/SiO_2$ interface. No difference was obtained when comparing the DBRs of these two device classes under an optical microscope [see Figs. S1(b) and S1(d) as an example]. Since at the current stage there is no possibility to determine during the preparation process if the mirror broke at the $TiO_2/SiO_2$ interface, the samples must be characterized by reflectivity measurements after the cavity fabrication [e.g., Figs. 1(c) and 4(a)] to conclude whether the cavity wavelength is proper. In principle, the tuning range of the cavity wavelength and the accuracy of hitting a specific resonance wavelength can be increased by using higher or lower PMMA concentrations and smaller concentration steps, respectively. Furthermore, we check the polarization properties of our mechanically assembled cavities. In particular, we study the angle-dependent polarization splitting (referred to as TE/TM splitting), evolving from the angle-dependent phase delay of light

25 August 2023 08:16:52


Published under license by AIP Publishing

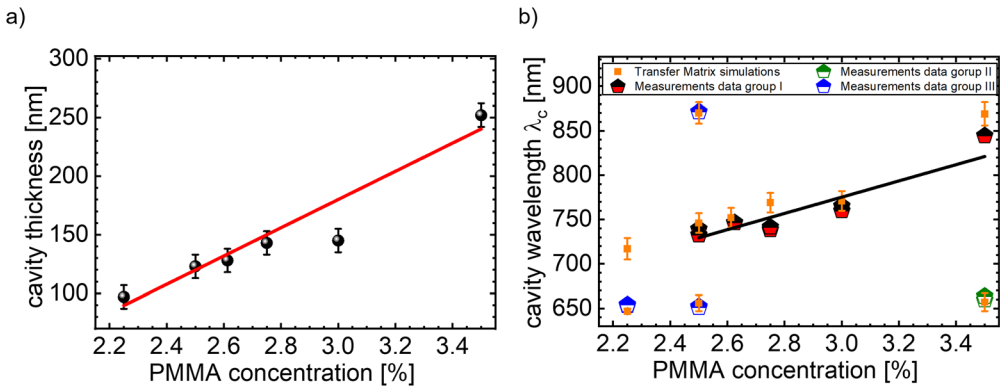


**FIG. 3.** (a) Measured thickness of the PMMA layer on $SiO_2$ reference samples. The red line is a guide to the eye. (b) Measured optical cavity wavelength (black, blue, and green dots) and transfer matrix simulations (orange). Input parameters are the measured thicknesses from (a) and the refractive index of PMMA,[13] $SiO_2$, and $TiO_2$.[14,15] The layer thicknesses of $SiO_2$ and $TiO_2$ are 129 and 79 nm, resulting in a DBR stop band centered at 750 nm. The black line is a guide to the eye. The deviating data result from a higher longitudinal mode (green, data group II) as well as inaccuracies during mechanical fragmentation of the top DBR (blue, data group III).

reflected at a dielectric mirror.[12] This polarization phenomenon, which strongly depends on the angle of incident and reflected light, is a core enabling feature for advanced experiments dedicated to the study of topological phenomena and spin–orbit coupling of light in microcavities.[16–19] Figure 4(a) displays a reflectivity spectrum of a cavity with 3.5% PMMA concentration, which is clearly characterized by two optical resonances with a degenerate energy at $k = 0$. As expected, the splitting scales approximately as $\theta^2$ for small incident angles $\theta$ and, therefore, as $k^2$ for small in-plane wave vectors[12] $k$ [Fig. 4(b)]. The magnitude of the TE/TM

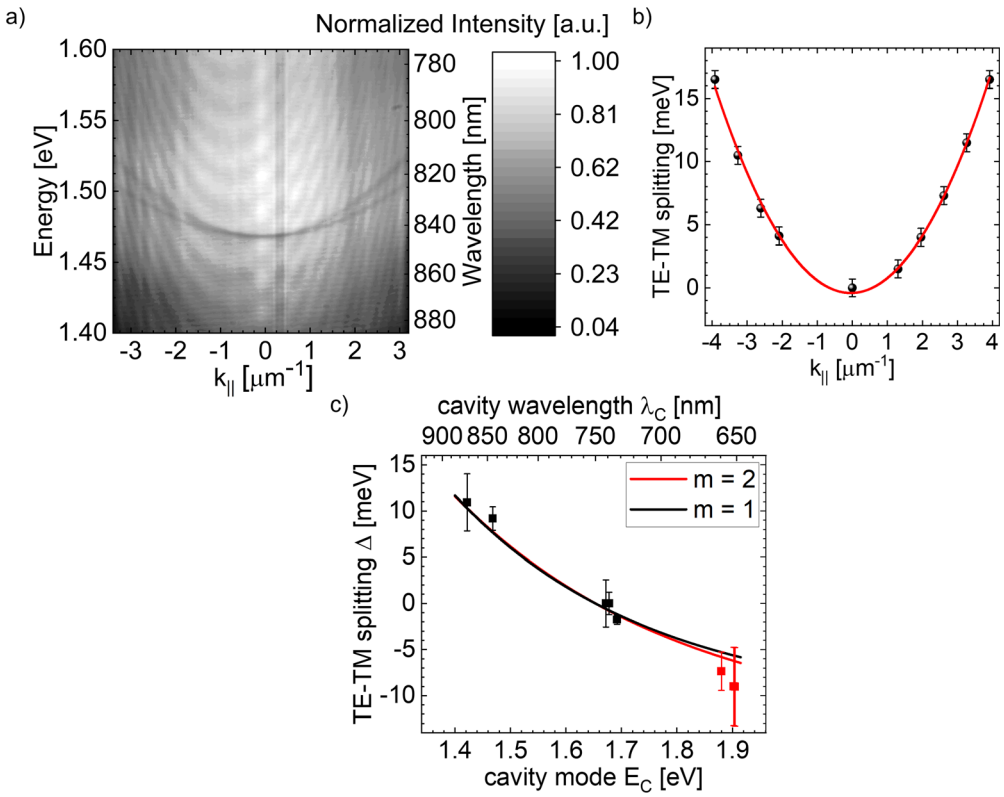


**FIG. 4.** (a) Energy-momentum dispersion of a cavity with 3.5% PMMA concentration and large TE-TM splitting. (b) TE-TM splitting extracted from (a) and parabolic fit (red). (c) TE-TM splitting at $k_{||} = (3.1 \pm 0.1)\ \mu m^{-1}$ for cavities with different PMMA concentrations and, hence, cavity wavelengths. The black (red) line corresponds to an analytical model for the fundamental mode ($m = 1$) and a higher longitudinal mode ($m = 2$).[12]

25 August 2023 08:16:52


Published under license by AIP Publishing

splitting depends on a variety of factors but most notably on the deviation of the cavity energy (determined by the thickness and refractive index of the cavity) from the central frequency of the DBR stop band (1.653 eV).[12] This behavior is well reflected in Fig. 4(c), where we plot the magnitude of the TE/TM splitting as a function of the cavity mode energy. Indeed, for a cavity energy close to $k_{||} = 0\,\mu\text{m}^{-1}$, the TE/TM splitting approaches zero while reaching very large values ~10 meV for the case of significant deviations from the Bragg condition. The black (red) line corresponds to an analytical model for the Fabry–Pérot mode $m = 1(\text{m} = 2)$ defined by the cavity wavelength $\lambda_c = 2n_c d_c/m$, the thickness $d_c$, and the refractive index $n_c$ described in Ref. 12. The simulation depends on the stop band center, $n_c = 1.47$, the refractive index of $TiO_2$ ($n_{TiO_2} = 2.35$) as well as $SiO_2$ ($n_{SiO_2} = 1.45$), and $k_{||} = 3.25\,\mu\text{m}^{-1}$. The refractive indices were assumed to be constant in the relevant energy region. More details can be found in the supplementary material. Since we did not adapt the thickness of the DBR mirrors, any modification of the cavity spacer thickness directly translates to a shift of the mode away from the cavity center.

Finally, we discuss a PMMA-free approach for the mechanical assembly of an all-dielectric monolithic microcavity. Here, a sacrificial polypropylene-carbonate (PPC) film, commonly used for stacking of van der Waals heterostructures,[20] is spin-coated on top of a PDMS stamp stabilized by a microscope slide. After picking up a DBR fragment with the prepared PDMS/PPC stamp, half of the cavity spacer is deposited by radio frequency (RF) magnetron sputtering of $SiO_2$ [see Fig. 5(a), left]. This is a prominent PVD method for making high-quality optical coatings, which enables a higher degree of control over the thickness of the $SiO_2$ cavity spacer compared to spin coating PMMA.

The top half of the microcavity consisting of the DBR and the sputtered top half of the $SiO_2$ cavity spacer is placed onto the bottom half consisting of a DBR, the bottom-half of the $SiO_2$ cavity spacer, and a TMDC monolayer, by employing a house-built stacking stage with an integrated heating module [see Fig. 5(a) right]. The stage allows us to align the DBR chip well with the monolayer region. After bringing the DBR chip in contact with the DBR substrate, the PPC film with the DBR chip separates from the PDMS at $T = 130\,^{\circ}C$,[6] and the assembly of the all-dielectric microcavity is achieved [see Fig. 5(b)].

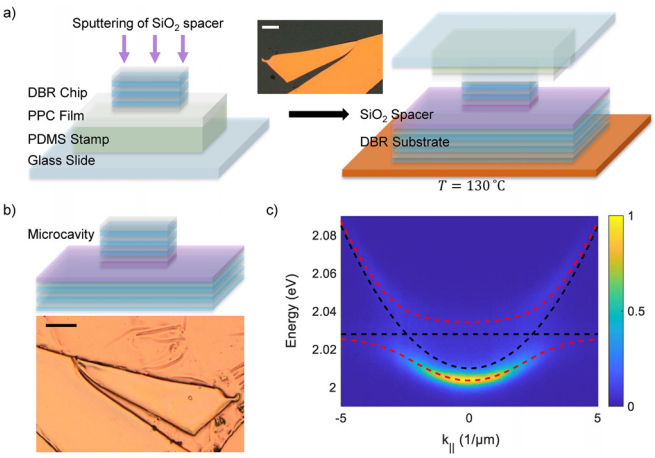


**FIG. 5.** (a) Schematic assembly process of an all-dielectric monolithic microcavity without PMMA. A $SiO_2$ spacer (deposited by RF magnetron sputtering) on top of a DBR chip is placed on a sacrificial poly-propylene carbonate (PPC) film, and the microcavity is assembled with a van der Waals stacking stage. (b) Schematic diagram and microscope image of an assembled microcavity. (c) Angle-resolved photoluminescence spectrum of an all-dielectric microcavity with an integrated $WS_2$ monolayer. The red (black) dashed lines correspond to the polariton modes (cavity and exciton resonances). The scale bar sizes in (a) and (b) are 50 $\mu$m.

An angle-resolved photoluminescence spectrum of such a microcavity with an integrated monolayer $WS_2$ is presented in Fig. 5(c). The emission from this structure fits well to the lower and the upper polariton dispersion branches, with a Rabi-splitting of 25 meV and a detuning between the exciton and the cavity resonances of −18 meV. Hence, the mechanically assembled all-dielectric optical microcavity operates in the strong coupling regime between the $WS_2$ excitons and the cavity photons. Since this approach does not require any material deposition on top of the TMDC monolayers, the optical properties of the integrated monolayers are fully preserved, which enables a high performance of the polaritons in the final device.

In summary, our paper details a low-cost approach to the fabrication of high quality factor microcavities based on micromechanical assembly. Our technique is inspired by the dry PDMS transfer method for TMDC fabrication. We utilize commercially available DBRs and a house-built transfer microscope as technology tools. We believe that this technique can be used by small and medium size teams without access to the sophisticated and expensive coating infrastructure to explore the field of cavity quantum electrodynamics with atomically thin crystals.

See the supplementary material for microscope images of an exfoliated mirror on PDMS and PMMA, examples of dirt on the surface of the mirror, and DBR pieces terminated with $TiO_2$ and $SiO_2$, respectively. It also includes further details about the TE-TM model and the polariton model from Fig. 2(b).

We acknowledge support from the state of Bavaria. C.S. acknowledges support from the European Research Commission (Project unLiMIt-2D, Grant No. 679288). M.W., E.E, and E.A.O. acknowledge support from the Australian Research Council (Grant No. CE170100039). Useful discussions with C. Anton-Solanas are acknowledged. P.S and M.R. are supported by the French National Research Agency (IDEX program ANR-15-IDEX-02, and research Grant No. ANR-16-CE30-0021). The data are available from Christian Schneider upon reasonable request.

## REFERENCES

[1] C. Schneider, M. M. Glazov, T. Korn, S. Höfling, and B. Urbaszek, Nat. Commun. **9**, 2695 (2018).
[2] L. C. Flatten, Z. He, D. M. Coles, A. A. P. Trichet, A. W. Powell, R. A. Taylor, J. H. Warner, and J. M. Smith, Sci. Rep. **6**, 33134 (2016).
[3] N. Lundt, S. Klembt, E. Cherotchenko, S. Betzold, O. Iff, A. V. Nalitov, M. Klaas, C. P. Dietrich, A. V. Kavokin, S. Höfling, and C. Schneider, Nat. Commun. **7**, 13328 (2016).
[4] X. Liu, T. Galfsky, Z. Sun, F. Xia, E. C. Lin, Y. H. Lee, S. Kéna-Cohen, and V. M. Menon, Nat. Photonics **9**, 30 (2015).
[5] H. G. Kim and H. B. R. Lee, Chem. Mater. **29**, 3809 (2017).
[6] M. Wurdack, T. Yun, E. Estrecho, N. Syed, S. Bhattacharyya, M. Pieczarka, A. Zavabeti, S.-Y. Chen, B. Haas, J. Müller, M. N. Lockrey, Q. Bao, C. Schneider, Y. Lu, M. S. Fuhrer, A. G. Truscott, T. Daeneke, and E. A. Ostrovskaya, Adv. Mater. **33**, 2005732 (2021).

25 August 2023 08:16:52


Published under license by AIP Publishing

[7]H. Knopf, N. Lundt, T. Bucher, S. Höfling, S. Tongay, T. Taniguchi, K. Watanabe, I. Staude, U. Schulz, C. Schneider, and F. Eilenberger, Opt. Mater. Express **9**, 598 (2019).
[8]C. Rupprecht, M. Klaas, H. Knopf, T. Taniguchi, K. Watanabe, Y. Qin, S. Tongay, S. Schröder, F. Eilenberger, S. Höfling, and C. Schneider, Opt. Express **28**, 18649 (2020).
[9]A. Castellanos-Gomez, M. Buscema, R. Molenaar, V. Singh, L. Janssen, H. S. J. Van Der Zant, and G. A. Steele, 2D Mater. **1**, 011002 (2014).
[10]C. W. Lai, N. Y. Kim, S. Utsunomiya, G. Roumpos, H. Deng, M. D. Fraser, T. Byrnes, P. Recher, N. Kumada, T. Fujisawa, and Y. Yamamoto, Nature **450**, 529 (2007).
[11]N. Lundt, M. Klaas, E. Sedov, M. Waldherr, H. Knopf, M. Blei, S. Tongay, S. Klembt, T. Taniguchi, K. Watanabe, U. Schulz, A. Kavokin, S. Höfling, F. Eilenberger, and C. Schneider, Phys. Rev. B **100**, 121303 (2019).
[12]G. Panzarini, L. C. Andreani, A. Armitage, D. Baxter, M. S. Skolnick, V. N. Astratov, J. S. Roberts, A. Kavokin, M. Vladimirova, and M. A. Kaliteevski, Phys. Rev. B **59**, 5082 (1999).
[13]G. Beadie, M. Brindza, R. A. Flynn, A. Rosenberg, and J. S. Shirk, Appl. Opt. **54**, F139 (2015).
[14]L. Gao, F. Lemarchand, and M. Lequime, Opt. Express **20**, 15734 (2012).
[15]S. Sarkar, V. Gupta, M. Kumar, J. Schubert, P. T. Probst, J. Joseph, and T. A. F. König, ACS Appl. Mater. Interfaces **11**, 13752 (2019).
[16]N. Lundt, Ł. Dusanowski, E. Sedov, P. Stepanov, M. M. Glazov, S. Klembt, M. Klaas, J. Beierlein, Y. Qin, S. Tongay, M. Richard, A. V. Kavokin, S. Höfling, and C. Schneider, Nat. Nanotechnol. **14**, 770 (2019).
[17]A. Kavokin, G. Malpuech, and M. Glazov, Phys. Rev. Lett. **95**, 136601 (2005).
[18]C. Leyder, M. Romanelli, J. P. Karr, E. Giacobino, T. C. H. Liew, M. M. Glazov, A. V. Kavokin, G. Malpuech, and A. Bramati, Nat. Phys. **3**, 628 (2007).
[19]A. Gianfrate, O. Bleu, L. Dominici, V. Ardizzone, M. De Giorgi, D. Ballarini, G. Lerario, K. W. West, L. N. Pfeiffer, D. D. Solnyshkov, D. Sanvitto, and G. Malpuech, Nature **578**, 381 (2020).
[20]L. Wang, I. Meric, P. Y. Huang, Q. Gao, Y. Gao, H. Tran, T. Taniguchi, K. Watanabe, L. M. Campos, D. A. Muller, J. Guo, P. Kim, J. Hone, K. L. Shepard, and C. R. Dean, Science **342**, 614 (2013).

25 August 2023 08:16:52


Published under license by AIP Publishing